Identifying Chemical Functionalization on Individual Carbon Nanotubes and Graphene by Local Vibrational Fingerprinting

Laura Zuccaro,[†] Klaus Kern,[†,§] and Kannan Balasubramanian*[,†]

[†]Max Planck Institute for Solid State Research, Heisenbergstrasse 1, D-70569 Stuttgart, Germany and [§]Institut de Physique de la Matière Condensée, Ecole Polytechnique Fédérale de Lausanne, CH-1015 Lausanne, Switzerland

ABSTRACT Chemical functionalization of carbon nanotubes (CNTs) and graphene allows for fine-tuning their physical and chemical properties to realize fascinating new fundamental phenomena as well as exotic applications. A primary challenge in such endeavors is the need to identify the chemical nature of attached functionalities at a single-nano-object level in a spatially resolved manner. Here we report the vibrational fingerprinting of functional groups that are attached to individual CNTs and graphene flakes. In order to achieve this, we decorate noncovalently functionalized CNTs and graphene with nanoparticles, which leads to the appearance of Raman peaks that can be correlated with the vibrational modes characteristic of the functional groups with diffraction-limited spatial resolution. The presented strategy is generic enough to be extended to other chemical modification routes on a range of nanostructures and hence will allow for rapid characterization of chemical modification of individual (semi)conducting nanostructures.

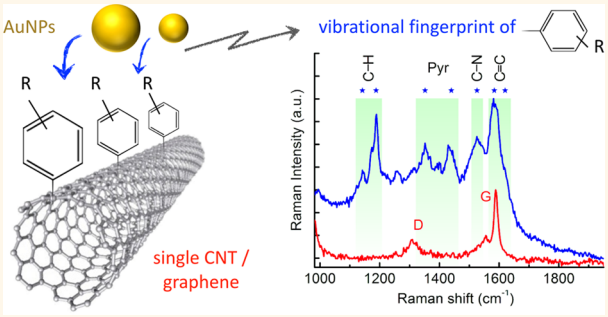

KEYWORDS: Raman spectroscopy · SERS · pyrrole · aniline · noncovalent · chemical modification · carbon · nanostructures

Chemical functionalization of nanostructures is fundamentally important for obtaining new physical and chemical properties and for engineering the nanostructures for desired applications.[1] For example, by chemically modifying carbon nanotubes (CNTs) a range of electronic devices including transistors and sensors have been demonstrated.[2−4] Chemical functionalization strategies are being vigorously explored for modifying the magnetic and electronic properties of graphene, for example, to realize a band gap.[5−8] In almost all of these functionalization methods, chemical information about the attached moieties is not available on a local scale or on a single object level, for example on individual CNTs on insulating substrates. On bulk samples, containing a large amount of CNTs, X-ray photoelectron spectroscopy (XPS) has been widely used to obtain some chemical information after functionalization.[9−11] Similarly on large graphene flakes (in mm range) it is possible to use XPS to obtain chemical information on the attached species.[9] However, even here, due to the rather large size of the X-ray beam (typically in the range 0.1−10 mm), high sensitivity and spatial resolution are hardly achievable in probing the chemical functionalities.[12,13] Recently, nanoscale X-ray imaging is opening avenues for obtaining chemical information down to 30 nm resolution.[14,15] In many other cases we only have indirect information about the groups, such as by the observation of expected changes in physical and chemical properties.[16−18] In this context, one fundamental question that cannot be answered yet is if the attached moieties are chemically intact or, in other words, are the functional groups really preserved after a certain functionalization strategy especially when working with individual nanostructures.

Here we present for the first time a way to resolve this fundamental question by systematically obtaining chemical information about the attached moieties on individual

* Address correspondence to b.kannan@fkf.mpg.de.

Received for review January 22, 2015 and accepted March 3, 2015.

Published online March 03, 2015
10.1021/acsnano.5b00479

nano-objects. Utilizing the electropolymerization of pyrrole or aniline on carbon nanostructures as candidate models, we demonstrate that we can identify the functional groups in a spatially resolved manner. The principle is based on the detection of Raman spectra of the attached moieties. The intensities of the Raman-active modes (which are otherwise almost unobservable at submonolayer coverages) are significantly enhanced through the additional attachment of gold nanoparticles (AuNPs) by surface-enhanced Raman scattering processes (SERS).[19,20] We bring these AuNPs selectively on the nanotube or graphene surface through a versatile electrodeposition approach.[19,21,22] This ensures a good signal-to-baseline ratio (in the range 1.2 to 10), providing spectroscopic information about the attached moieties exclusively on the CNTs/graphene with a very high fidelity. SERS substrates comprising roughened metal surfaces or nanoparticle arrays have been widely reported to have high sensitivity with the capability to detect even single molecules.[23−25] By combining SERS with super-resolution microscopy, the position of single emitters could be determined with a precision better than 5 nm.[26] On the other hand, tip-enhanced Raman spectroscopy (TERS) is emerging as a powerful technique[27] with the promise of routinely obtaining chemical information with high spatial resolution (down to 1.7 nm[28]) on various surfaces including CNTs and graphene.[29−36] Moreover, Raman modes of individual dye molecules with submolecular resolution under ultra-high-vacuum conditions have also been observed by utilizing tip-induced plasmonic enhancement.[37] In the literature, a number of examples of using TERS for the spatially resolved investigation of various physical and chemical aspects are available, such as identification of different CNTs in a bundle, effect of pressure on the Raman modes, and localization of defects, edges, contaminants, *etc.*[38−42] Local vibrational information in the form of infrared absorption spectra is attainable also using nano-FTIR[43] or tip enhancement with resolution down to 25 nm.[44] There is however no demonstration yet of the use of TERS or SERS or infrared spectroscopy to systematically identify the vibrational modes of controllably deposited chemical functionalities on individual CNTs or graphene in a spatially resolved manner. In contrast to other techniques, the use of electrodeposition to obtain AuNPs directly on the chemical functionalities ensures an intimate coupling between the two, thereby promising a very high Raman enhancement (around 2 orders of magnitude).[19,45] While there exist various demonstrations of detecting analyte molecules deposited on AuNPs, there is no report yet on the possibility to obtain spatially resolved chemical information on controllably attached functional groups on individual carbon nanotubes or graphene. Moreover, the strategy presented here for the detection of vibrational modes can be implemented using a standard confocal Raman microscope without the need for an expensive and elaborate instrument (such as a TERS microscope).

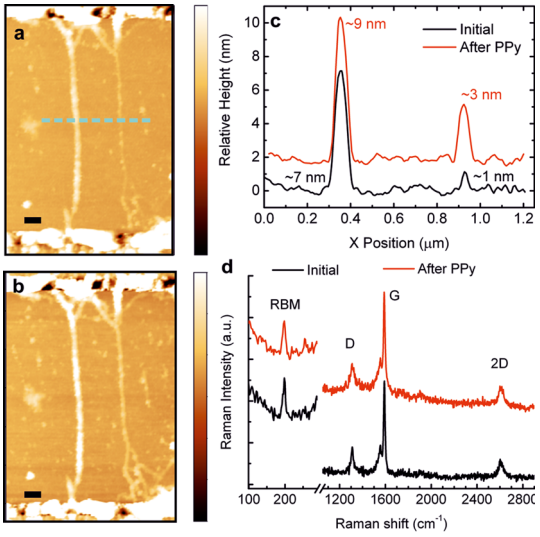

Figure 1. Noncovalent functionalization of individual CNTs. (a, b) AFM images of individual CNT bundles in an electrode gap before (a) and after (b) electropolymerization with pyrrole: *z*-scale bar: 40 nm, *x,y*-scale bar: 200 nm. (c) Line profile along the cyan line in (a) showing the relative heights of the nanotubes before and after electropolymerization. The profiles are shifted for clarity. (d) Raman spectrum on the thinner right tube before and after electropolymerization, showing the radial breathing mode (RBM), the D-peak, G-band, and 2D-peak of the CNT on the right side (λ_{ex}: 633 nm, 0.4 mW, 2 × 5 s).

RESULTS AND DISCUSSION

Typically for carbon nanostructures a covalent attachment of functional groups can be deciphered through changes in the relative intensity of the D-peak.[46,47] Here we focus on the more challenging task of obtaining chemical information after noncovalent attachment of a small quantity of functional moieties, which in general does not affect the Raman signature of the underlying nanostructure. We first present the effect of noncovalent functionalization on individual CNT bundles. Figure 1a shows an AFM image of two bundles of CNTs assembled in an electrode gap. After initial characterization, the CNTs are coated with a polypyrrole (PPy) layer through electropolymerization of pyrrole (see Methods). This is a versatile method in which the surface of the CNTs can be decorated with PPy moieties selectively and has been successfully used on many occasions.[21,48−50] Figure 1b shows the AFM image after the modification and Figure 1c a line profile showing the increase in thickness of around 2 nm on both the tubes. Figure 1d shows Raman spectra of the thinner tube before and after attachment of PPy. It is apparent that the Raman spectrum has not changed significantly after the modification. Most importantly, the ratio of the Raman intensities of the D-peak to the G-peak (I_D/I_G) remains

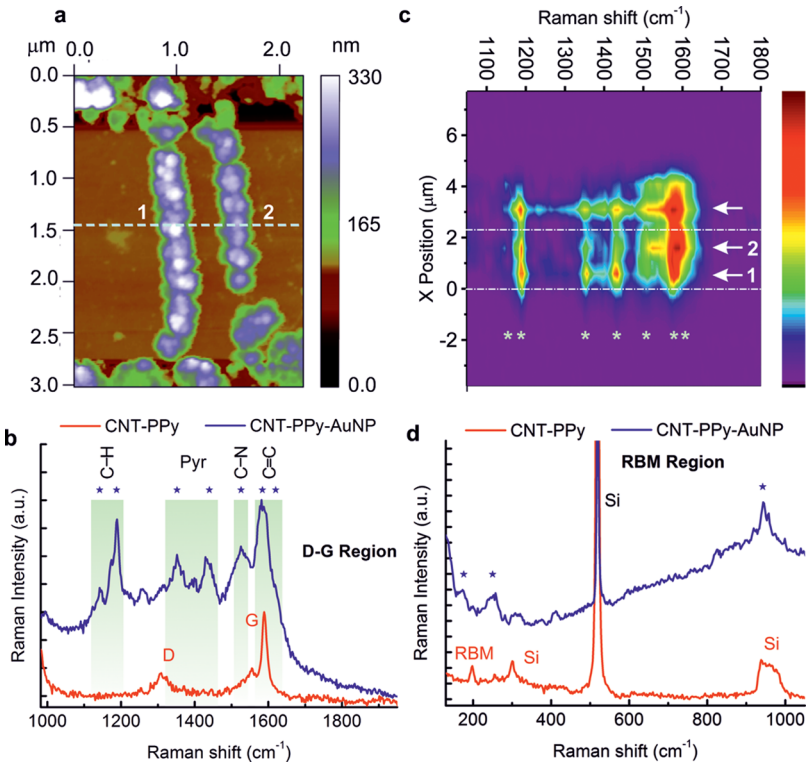

Figure 2. Vibrational fingerprinting of functionalized CNTs. (a) AFM image of the same sample as in Figure 1 after attachment of AuNPs on the polypyrrole (PPy)-functionalized CNTs (see Figure S1 for a zoomed-out view of this device and for height profiles). (b) Raman spectrum around the D- and G-peaks obtained on the right tube before and after the attachment of AuNPs. (c) Raman map along the cyan line in (a), where the Raman spectrum at each point is collected vertically as an image. The span of the horizontal line in (a) corresponds to the vertical region between the two white dashed lines in (b). The white arrows 1 and 2 mark the position of the two CNTs labeled correspondingly in (a). The third white arrow marks the Raman spectrum from a third CNT present also in the gap (see Figure S1). (d) Raman spectrum around the RBM obtained on the right tube before and after the attachment of AuNPs. Peaks marked with Si are because of the substrate due to silicon or silicon oxide (λ_{ex}: 633 nm, 0.4 mW, 2 × 5 s for CNT-PPy and 2 × 1 s for CNT-PPy-AuNP). The *'s correspond to the position of the Raman modes, arising only after the attachment of AuNPs, which are assigned to the PPy layer on the CNTs.

unaffected, signifying a noncovalent attachment of the functional groups onto the CNT surface.[2,47] Moreover, there is no indication of the presence of additional chemical groups in the Raman spectrum, although we see a clear and consistent increase in the thickness of the nanotubes from one sample to the other.

The next step constitutes the central part of the fingerprinting strategy, wherein we controllably bring in AuNPs exclusively on the modified nanotube surface using the same electrochemical modification strategy described above. Specifically, a metal salt ($KAuCl_4$) in an aqueous solution is reduced at negative overpotentials (see Methods).[21,51,52] Figure 2a shows an AFM image of the same device with nanoparticles. It is apparent that the nanotubes (and the electrodes) are exclusively decorated with nanoparticles. Most likely the thin PPy layer favors charge transfer with the metal salt leading to the formation of AuNPs. Figure 2b shows the Raman spectrum (in the region of D- and G-peaks) at the same location on the thinner tube before and after the addition of nanoparticles. Clearly new peaks appear in the Raman spectrum of the CNT-PPy-AuNP ensemble, which are distinctly different from the D- and G-peaks of the underlying CNTs. It is worth mentioning that in the absence of the PPy layer (with only AuNPs on CNTs) we do not observe these additional peaks.[45,52] We attribute these peaks to the vibrational modes of the PPy layer that is sandwiched between the CNTs and AuNPs. On the basis of literature data available for electropolymerized pyrrole, we can assign the various peaks to the C−H bending, pyrrole ring stretch (Pyr), C−N stretching, and C═C stretching modes of polypyrrole.[53,54] The presence of nanoparticles results in an enhanced absorption (*e.g.*, *via* the availability of plasmon resonances) of light, leading to a selective enhancement of the Raman signals of the PPy layer (around 1 order of magnitude; see Supporting Information). Moreover, the strength of this near-field enhancement correlates with the far-field plasmonic absorption profile of the nanoparticles,[55] as we have shown for the case of pristine graphene.[19] In addition to this electromagnetic effect, chemical enhancement may also play a significant role in the emergence of these new Raman peaks.[56] (The details about the relative contributions of these effects to the Raman enhancement will be a subject of future investigation.) Figure 2c shows a Raman map of the CNT-PPy-AuNP hybrid along the dashed line in

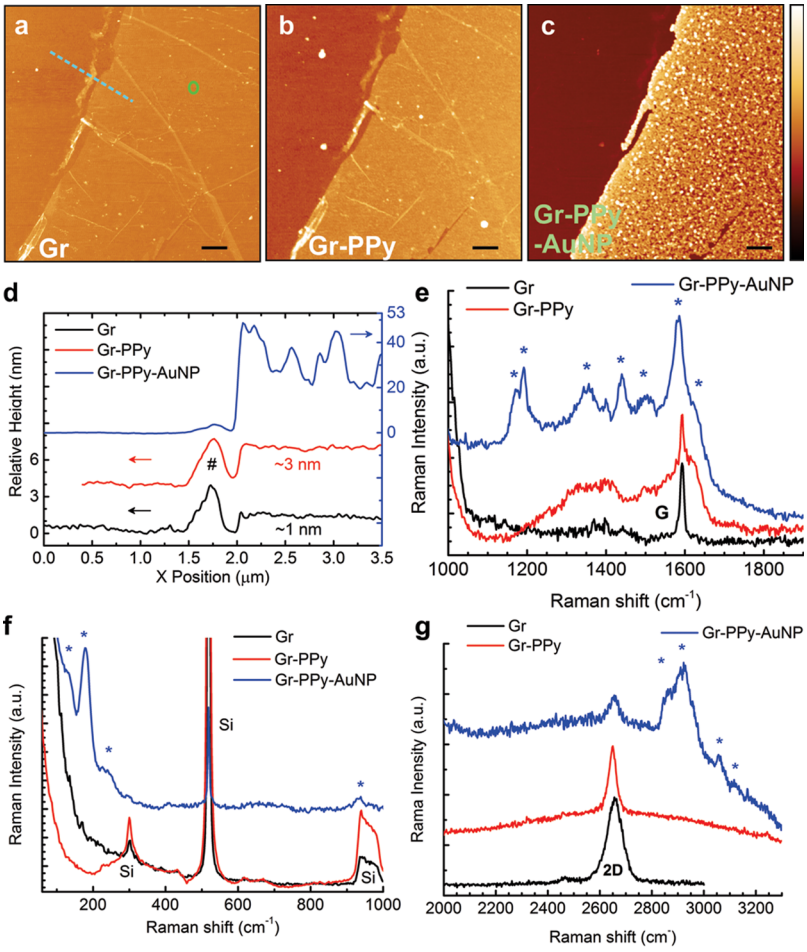

Figure 3. Vibrational fingerprinting of functionalized graphene. (a−c) AFM images before (a) and after electropolymerization with PPy (b) and after subsequent attachment of AuNPs (c). *z*-Scale bar is 22 nm in (a) and (b), while it is 70 nm in (c); *x*,*y*-scale bar is 1 μm. (d) Line profile along the cyan line in (a) before and after PPy and AuNP decoration. The profiles are shifted for clarity. # refers to a small graphene region that is not in contact with the electrode and hence remains unmodified. The height of this region serves as a good internal control. (e−g) Raman spectra compared at different stages of functionalization, measured in three different spectral regions (split into three regions for clarity) at the spot shown in (a). The peaks marked by * are attributed to the PPy layer on graphene (λ_{ex}: 633 nm, [4 mW, 2 × 5 s] for Gr and Gr-PPy, [0.4 mW, 6 × 1s] for Gr-PPy-AuNP).

Figure 2a, where it can be seen that the same vibrational fingerprint (marked by *) is observable on all the CNTs present in the gap (note that there is another CNT close by; see Figure S1). The relative intensity of a certain mode is however different on the three tubes in this device. This can be understood by considering that the tubes have different reactivities, and hence the thickness of the PPy layer and the density of AuNPs vary from one tube to another. Figure 2d presents the Raman spectrum in the region around the radial breathing mode (RBM), where we see three additional peaks, which were not present on the pristine CNTs (the assignment of these peaks will be discussed below). It is worth mentioning that we carefully choose the conditions for depositing the AuNPs, in order not to disturb the chemical structure of the underlying polymer during electrodeposition. For this purpose, we never use a potential below −0.3 V *vs* Ag/AgCl, under which conditions the polymeric layer is known to be resistant to any persistent chemical change. (In order to induce irreversible reduction in polypyrrole, we need a potential lower than −0.6 V *vs* Ag/AgCl.)[53,57−59] Continuous recording of the Raman spectra on the CNT-PPy-AuNP ensemble confirms the persistence of these peaks. However, the Raman intensity decreases with time (see Figure S2), pointing to the sensitivity of the polymer layer to high light intensities. By optimizing the acquisition conditions (*e.g.*, low power of 0.4 mW for very short acquisition times, typically 1 s pulses), we were able to obtain persistent and reproducible peaks from one sample to the other (see Figure S3).

Before we go to a detailed analysis of the observed modes, we show that we can utilize the same strategy to observe the vibrational modes of chemical functionalization also on graphene. For this purpose commercially procured chemical vapor deposition (CVD)-grown graphene was transferred[60] onto Si/SiO_2 substrates with predefined electrode lines (see Methods). Figure 3a−c show AFM images of a typical graphene area at an initial stage, after electropolymerization of pyrrole, and

after attachment of AuNPs. From the line profile in Figure 3d we infer that we have a nominal thickness for the PPy layer of around 2 nm and the nanoparticles show heights in the range 20−50 nm. The Raman spectra obtained at the initial stage, after PPy, and after deposition of AuNPs are collected for three different spectral regions in Figure 3e−g. Graphene modified with PPy shows mainly the typical G- and 2D-peaks of graphene in addition to the substrate-related peaks in the low-frequency (<1000 cm^{-1}) region. Around the G-peak two broad bands are observed; however we do not see any clear peaks even up to a PPy-layer thickness of 10 nm. The addition of nanoparticles leads to the appearance of new peaks, whose origin is attributed to the sandwiched PPy layer. The various modes (represented by *) occur at rather similar frequencies to that of the PPy layer on CNTs (see also Figure S4 for similar spectra in other locations). These peaks are not observed in the absence of the polymeric layer.[19]

Now we turn toward the actual position of the peaks that were observed in most of the locations on graphene/CNTs (see also Table ST1 in the Supporting Information). Polypyrrole can exist predominantly in three forms: the neutral form, the polaronic radical cation form, and the bipolaronic dication form.[53] We first consider the assignment of the modes in the region around the G-peak as shown in Figure 3e. The various peaks can be classified into four sets: the C−H-related modes at 935 cm^{-1} (C−H wag) and 1160−1200 cm^{-1} (C−H bending), the ring stretching modes typical of pyrrole at around 1350 and 1440 cm^{-1}, C−N-related modes around 1500 cm^{-1}, and the C═C stretching modes around 1600 cm^{-1}.[53,54] The position of the weak C−H wag mode, the pyrrole characteristic ring stretching bands, and the appearance of the C═C stretching band beyond 1600 cm^{-1} indicate the predominant occurrence of the dication form of the polymer on graphene as well as on CNTs.[61,62] The C−H bending modes occur at higher frequencies than what is typical for polypyrrole. Taking this together with the position of the C−N stretching modes we conclude that we have most likely polymer chains of short conjugation length.[62,63] This is not surprising since we use a low overpotential for a short time in order to attain a low coverage on the carbon nanostructure surface.[64] Furthermore, we clearly see additional bands in the high-frequency region (2700−3300 cm^{-1}) around the graphene/CNT 2D-peak, which may be assigned to CH_2 stretching (in the range 2800−3150 cm^{-1}) and C═O-related modes (second harmonic at around 3230 cm^{-1}), respectively,[65,66] which are typically not reported for PPy. This signature (together with the peak at around 175 cm^{-1})[67] suggests that we most likely have an oxidized form of PPy, wherein the end groups of the polymer chain are converted to pyrrolidone, with the formation of a methylene and a carbonyl group.[68−70] Due to a low conjugation length, the relative proportion of such regions is higher (in comparison to bulk PPy), leading to a stronger signal in the Raman spectrum of our samples. Interestingly, we have seen this band also in samples that were not decorated with nanoparticles (with very thick PPy layers, >30 nm; see Figure S5), leading us to conclude that the electroreduction of gold does not create these functionalities.[68] The use of aqueous solvent may also have an effect on this oxidation of the end groups, which may be overcome partially using water-free organic solvents.[71] Here, we are limited to aqueous solvents because of fabrication limitations.

The electrodeposition of AuNPs on functionalized graphene or CNTs and the resulting Raman enhancement are sensitive to many factors. First, in order to attach AuNPs, the functional layer must not be very thick. Otherwise, the occurrence of electron transfer to the metal precursors is hampered, making it difficult or almost impossible to generate the AuNPs. Second, a certain degree of tuneability in the size and density of the AuNPs is necessary in order to routinely observe the Raman fingerprint of sandwiched functional layers. Typically small AuNPs at a high density are ideal for observing the best enhancement on graphene.[19] On CNTs, it is more favorable to have larger particles at a high density. Nevertheless, our electrodeposition strategy directly provides this tuneability through the modulation of electrochemical parameters.[19,51] This is also one of the reasons that we prefer electrodeposition to obtain the AuNPs, rather than a direct use of preprepared Au colloids. Au colloids may have other disadvantages such as the presence of stabilizing surfactants, whose Raman-active modes may hamper the unambiguous recording of the true vibrational fingerprint of the attached organic moieties.[72] Next, the occurrence of the graphene- or CNT-related peaks in their corresponding PPy-AuNP hybrids is a function of the thickness of the attached polymer layers. As the thickness increases, the electromagnetic and chemical coupling[19] between the AuNPs and graphene/CNT decreases, resulting in a relatively lower intensity of the RBM and D-, G-, and 2D-peaks *in comparison* to the peak intensities of the polymer layer (as in Figure 2d; note that graphene/CNT peaks do not completely disappear; there is mainly a reduction in the *relative* Raman intensity). Finally, we have attempted the removal of the AuNPs by etching in an acidified iodide solution. However, we have very often observed some contamination on the surface arising due to incomplete etching or reaction byproducts or additional chemical reactions with the functionalities. This suggests that we may not be able to reuse the sample after fingerprinting, similar to other surface characterization techniques such as X-ray/electron spectroscopy. Nevertheless, the reproducibility in the fingerprints

(Figures S3 and S4) indicates that we can deploy the method to reliably screen the chemical nature of functional groups obtainable from a specific functionalization protocol.

From the foregoing discussion it is apparent that our strategy provides a rich playground for obtaining information about the attached functional moieties on the CNTs/graphene in a very elaborate manner. In order to clearly assert that the observed modes are indeed characteristic of the attached functionalities, we have repeated the same procedure for another polymer, namely, polyaniline (PANI), obtained by electropolymerization of the aniline monomer at oxidative potentials.[48,49] Figure 4 presents the spectrum obtained on graphene-PANI-AuNP hybrids for the three different spectral regions and compares them directly with that of PPy. We can clearly identify a number of modes that are exclusively present on each of the two polymers, thereby confirming the capability of our method to fingerprint chemical functionalization on individual nanostructures (see Figure S4 for more spectra of graphene-PANI-AuNP).

We can take a closer look at the positions of the various modes of the graphene-PANI-AuNP hybrids (see also Table ST2 in the Supporting Information). Analogous to the case of PPy, we also see clear indications for the presence of low conjugation length of PANI from the peaks at 575 and 603 cm^{-1}.[73,74] PANI is generally composed of varying proportions of two basic units, namely, the quinoid and benzenoid forms.[75,76] The modes at 575 and 603 cm^{-1} in the low-frequency region are assigned to ring deformations of quinoid and benzenoid forms, respectively.[76] Furthermore, C−C/C═C stretching modes can be identified at around 1560 and 1625 cm^{-1} for the quinoid form and the phenyl rings, respectively.[73] The occurrence of both these two sets of modes indicates that we have both forms of PANI in the layer deposited on graphene. In many cases the relative peak intensities of the two forms are similar, although there is a slight variation from one location to the other. Moreover, at least two bands are observed in the vicinity of 1350 cm^{-1}, which arise from the C−N stretch characteristic of the polaronic nature of the polymer.[77] Along with the C−H bending mode at 1178 cm^{-1}, we can confirm that we predominantly have the polaronic emeraldine base form of polyaniline in our samples. The remaining band at around 1500 cm^{-1} and a mode at 409 cm^{-1} are assigned respectively to C═N stretching of imines and C═C stretch, respectively. Unlike in the case of PPy, we do not see any high-frequency modes or modes below 400 cm^{-1} for the obtained PANI layers, suggesting that we indeed have a chemically intact polymer layer typical of what is often reported in the literature on bulk samples. Accordingly, we have observed that the PANI layer on graphene is more stable than the PPy layer.

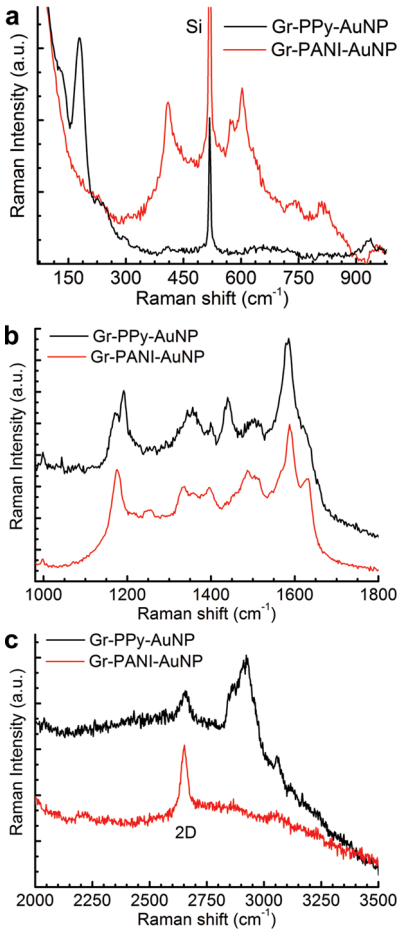

Figure 4. Comparison of vibrational fingerprints of PPy-modified and PANI-modified graphene. (a−c) Raman spectra obtained after attachment of AuNPs to polypyrrole (PPy)- and polyaniline (PANI)-modified graphene. The spectral regions are split into three for clarity. In the low (a) and high frequency (c) there is a clear difference in the two fingerprints. In the midfrequency region (b) although some peak positions are not different between the two cases (note that they are assigned to similar modes because of the similarity between PPy and PANI), the fingerprint is clearly distinct for the two cases (see also Figure S4). Si corresponds to peaks from the substrate due to silicon or silicon oxide, while 2D indicates the 2D-peak of graphene (λ_{ex}: 633 nm, 0.4 mW, 6 × 1 s).

On the basis of the success of our fingerprinting strategy, it is intriguing to look now for the spatial variation in the chemical functionalities that are attached to the carbon nanostructure surface. For this purpose, we have obtained Raman maps of PANI-functionalized graphene after the attachment of the AuNPs. Figure 5a shows a typical AFM image of a Gr-PANI-AuNP region, while Figure 5b shows the corresponding Raman map obtained by integrating the Raman intensities in the range 565−620 cm^{-1}. Figure 5c shows an overlay image of the AFM and Raman maps, where the origin of the signals can be clearly identified. It is apparent that the signal is strong at regions where there are big AuNPs or there is a high density.[19] At this stage, the variation in Raman intensity is strongly dominated by the distribution of the AuNPs

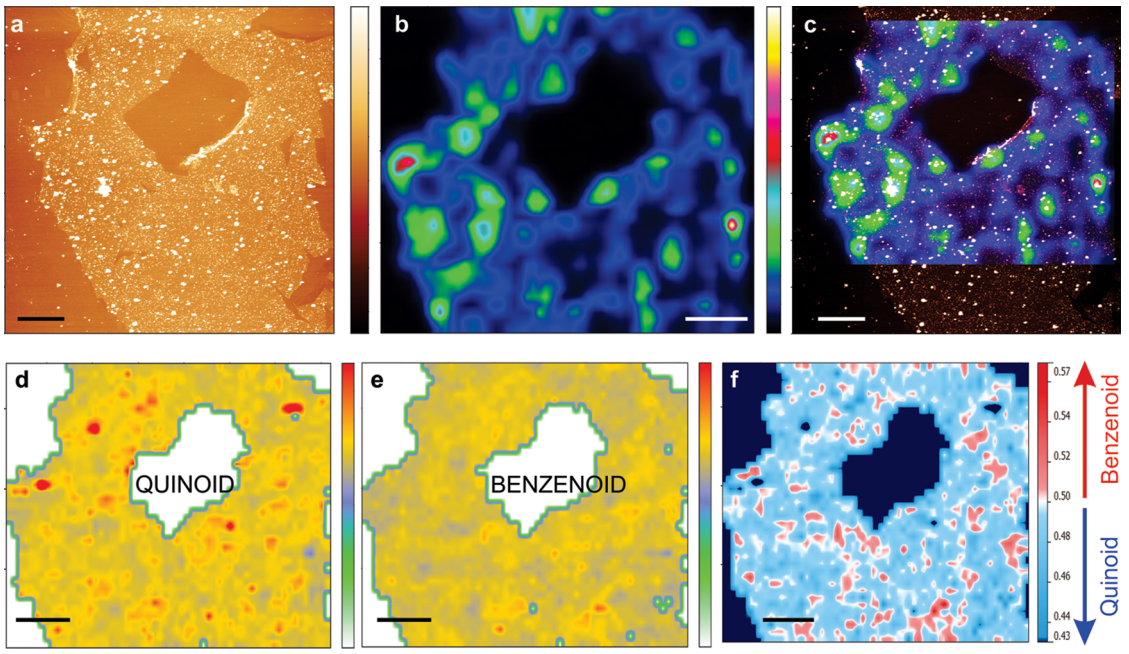

Figure 5. Spatial distribution of chemical functionalization on graphene. (a) AFM image of a graphene sheet after functionalization with polyaniline (PANI) and subsequent attachment of AuNPs. *z*-Scale bar is 75 nm (see Figure S6 for a zoomed-in view). (b) Raman map of the same area, where the Raman intensities in the range 565−620 cm^{-1} are integrated and plotted as a function of position (λ_{ex}: 633 nm, 0.4 mW, 3 × 1 s per point). (c) Overlay of images in (a) and (b) showing that the origin of high Raman intensity occurs at big particles or at high particle densities. (d, e) Raman maps showing the integrated intensities in the spectral ranges 566−588 and 595−617 cm^{-1}, corresponding to the modes of quinoid and benzenoid stretching of PANI, respectively. The intensities are from the Raman spectra of (b), but normalized to the baseline (around 700 cm^{-1}). (f) Spatial map of the relative proportion of benzenoid to quinoid forms of polyaniline obtained on graphene. 0.5 corresponds to an equal amount of both forms, while deviations from this value indicate a dominant occurrence of one form or the other as indicated by the red−cyan color scale. *x,y*-Scale bar is 5 μm in all images.

on the functionalized graphene surface. However, the nanoparticles themselves produce a broad background due to the fluorescence arising from a strong plasmonic absorption. We use this spatially varying baseline to correct the spectrum at every pixel to arrive at the normalized Raman maps for the quinoid (566−588 cm^{-1}) and benzenoid (595−617 cm^{-1}) forms of the PANI layer on graphene shown in Figure 5d and e (see Supporting Information for details of normalization). It is apparent that except for a few regions the Raman intensities from the quinoid or benzenoid forms are rather uniform over the entire investigated area, consistent with a homogeneous thickness observed in AFM images. However, the major advantage of our technique is that we can estimate the relative proportion of one kind of moiety with respect to the other. For PANI, the proportion of quinoid-to-benzenoid forms is typically expressed in the form of $([Q]_y:[B]_{1-y})_n$, with Q and B referring to quinoid and benzenoid, respectively).[73] On the basis of the measured Raman intensities and assuming a similar cross-section for these two modes (since they are very close), we can estimate the parameter *y* as a function of position. Figure 5f presents the spatial variation of this parameter *y*, where it is apparent that we have mostly 0.5 (corresponding to emeraldine), with slight deviations for benzenoid or quinoid forms. With this we have clearly exemplified the power of this fingerprinting strategy for the local identification of chemical functionalities on nanostructured surfaces.

CONCLUSIONS

In conclusion, we have presented a versatile strategy to obtain chemical information on thin layers of functional groups on nanostructured surfaces with diffraction-limited spatial resolution (see Figure S7). The key advantage of the proposed methodology is the possibility to obtain spatially resolved information about the chemical functionalities on individual nanostructures in an inexpensive manner (without the need for more expensive instruments such as TERS, or nano-IR spectroscopies, or synchrotron radiation). With respect to the type of nanostructures, the main restriction of the methodology is the necessity to obtain metallic nanoparticles on or around the functional groups. While this can be achieved in a straightforward manner on contacted 1D or 2D metallic or semiconducting[78] nanostructures, other types of nanostructures (polymeric/insulating/0D) may require alternative methods such as electroless deposition. On the other hand, the technique is generic enough to be extended to other functionalization routes. Moreover, the possibility to obtain spatial information about the chemical functionalities will allow for a rational evaluation or

rapid screening of the various functionalization schemes for a specific application. This advance is expected to open up a broad range of investigations on the fundamental and thorough understanding of chemical functionalization on nanostructures at a single-object level.

METHODS

Samples. Carbon nanotube devices were prepared by dielectrophoresis of purified HiPco single-wall CNTs (Unidym Inc.) dispersed in aqueous 0.1% Triton-X-100.[79] For this purpose, chips were prepatterned with Ti/Pt electrodes using photolithography. In order to realize graphene devices, commercially available CVD-graphene-on-copper was procured from Graphene Supermarket Inc. Subsequently graphene was transferred onto the chips by using polystyrene as polymer support and after etching the underlying copper in a solution of concentrated HCl with added H_2O_2. The polystyrene was removed by copious washing in toluene. Both CNT and graphene samples were annealed at 585 °C for 1 min in an argon atmosphere to get rid of organic contaminants.

Instruments. AFM images were obtained with a commercial Dimension V working in tapping mode in the ambient. Raman spectra were obtained on a LabRam HR equipped with an 800 mm monochromator, a 600 l/mm grating, a HeNe laser with an excitation wavelength of 632.8 nm, a 100× (NA 0.6) or a 50× (NA0.65) objective, and a detection pinhole of 100 or 140 μm. The power was maintained at 4 mW for acquisitions on bare CNTs or on bare graphene. In all other cases, a power of 0.4 mW was used in order not to degrade the polymer layer. The Raman spectra were measured and processed using LabSpec 5, and peak fitting was done using Origin 9.1. The Raman maps and AFM images were processed using Gwyddion. Electrochemical modification and measurements were performed using either an Ivium Compactstat or a Solartron 1285 potentiostat.

Electropolymerization with PPy/PANI; Attachment of Au Nanoparticles. The electrochemical modification of CNTs or graphene was performed in a small cell made out of poly(dimethylsiloxane) with a maximum volume of 50 μL, provided with Pt counter and Ag/AgCl reference electrodes (WPI Inc.). A probe needle was used to contact the electrode lines that were connected to CNTs/graphene. For electropolymerization, either 10 mM pyrrole or 10 mM aniline was used in water with added 0.1 M lithium perchlorate as supporting electrolyte. The electropolymerization took place while scanning the potential (cyclic voltammetry) to a maximum of 0.8 V (*vs* Ag/AgCl) for two cycles.[21] Subsequently the samples were rinsed with water and used for Raman measurements. Following this, the nanoparticle decoration was carried out potentiostatically by applying a chosen voltage for 20 s in an aqueous solution of 0.2 mM $KAuCl_4$ with 0.1 M lithium perchlorate as supporting electrolyte. The lowest potential used was −0.3 V *vs* Ag/AgCl. In the event of insufficient Raman signals from the polymer, the nanoparticle decoration was repeated by varying the voltage and fixing all other parameters, in order to obtain an optimal density and size of nanoparticles.[19] Please note that the Raman spectra were acquired immediately after the nanoparticle decoration. Spectra measured more than 1 day after the AuNP electrodeposition showed stronger signs of degradation and the quality of the Raman signals was sometimes poor.

Conflict of Interest: The authors declare no competing financial interest.

Supporting Information Available: Detailed AFM images of vibrational fingerprinting on CNTs and graphene, time evolution of Raman fingerprint signals on CNTs, Raman spectra from various samples showing the high reproducibility in obtaining the vibrational fingerprints, estimation of spatial resolution in Raman maps, and a table showing the assignments of the various Raman modes. This material is available free of charge *via* the Internet at http://pubs.acs.org.

Acknowledgment. We thank Yvonne Link and Stephan Schmid for help with metal deposition. We acknowledge the support of Mathieu Le Tacon, Matthias Hepting, and Jürgen Smet for access to Raman measurements.

REFERENCES AND NOTES

1. Maiti, U. N.; Lee, W. J.; Lee, J. M.; Oh, Y.; Kim, J. Y.; Kim, J. E.; Shim, J.; Han, T. H.; Kim, S. O. 25th Anniversary Article: Chemically Modified/Doped Carbon Nanotubes & Graphene for Optimized Nanostructures & Nanodevices. *Adv. Mater.* **2014**, *26*, 40–67.
2. Balasubramanian, K.; Burghard, M. Chemically Functionalized Carbon Nanotubes. *Small* **2005**, *1*, 180–192.
3. Burghard, M. Electronic and Vibrational Properties of Chemically Modified Single-Wall Carbon Nanotubes. *Surf. Sci. Rep.* **2005**, *58*, 1–109.
4. Singh, P.; Campidelli, S.; Giordani, S.; Bonifazi, D.; Bianco, A.; Prato, M. Organic Functionalisation and Characterisation of Single-Walled Carbon Nanotubes. *Chem. Soc. Rev.* **2009**, *38*, 2214–2230.
5. Hirsch, A.; Englert, J. M.; Hauke, F. Wet Chemical Functionalization of Graphene. *Acc. Chem. Res.* **2013**, *46*, 87–96.
6. Mao, H. Y.; Lu, Y. H.; Lin, J. D.; Zhong, S.; Wee, A. T. S.; Chen, W. Manipulating the Electronic and Chemical Properties of Graphene *via* Molecular Functionalization. *Prog. Surf. Sci.* **2013**, *88*, 132–159.
7. Hu, Y.; Sun, X. Chemically Functionalized Graphene and Their Applications in Electrochemical Energy Conversion and Storage. In *Advances in Graphene Science*; Aliofkhazraei, M., Ed.; INTECH, 2013.
8. Liu, J. Q.; Tang, J. G.; Gooding, J. J. Strategies for Chemical Modification of Graphene and Applications of Chemically Modified Graphene. *J. Mater. Chem.* **2012**, *22*, 12435–12452.
9. Choudhury, D.; Das, B.; Sarma, D. D.; Rao, C. N. R. XPS Evidence for Molecular Charge-Transfer Doping of Graphene. *Chem. Phys. Lett.* **2010**, *497*, 66–69.
10. Zhang, W. H.; Nefedov, A.; Naboka, M.; Cao, L.; Woll, C. Molecular Orientation of Terephthalic Acid Assembly on Epitaxial Graphene: NEXAFS and XPS Study. *Phys. Chem. Chem. Phys.* **2012**, *14*, 10125–10131.
11. Wepasnick, K. A.; Smith, B. A.; Bitter, J. L.; Fairbrother, D. H. Chemical and Structural Characterization of Carbon Nanotube Surfaces. *Anal. Bioanal. Chem.* **2010**, *396*, 1003–1014.
12. Kim, J. W.; Son, B.; Yu, H.; Park, H. M.; Lee, Y. S. The Use of Imaging XPS to Assess Ligand Binding to Nanoparticles. *Surf. Interface Anal.* **2014**, *46*, 193–196.
13. Hajati, S.; Tougaard, S. XPS for Non-Destructive Depth Profiling and 3D Imaging of Surface Nanostructures. *Anal. Bioanal. Chem.* **2010**, *396*, 2741–2755.
14. Sakdinawat, A.; Attwood, D. Nanoscale X-Ray Imaging. *Nat. Photonics* **2010**, *4*, 840–848.
15. Shapiro, D. A.; Yu, Y. S.; Tyliszczak, T.; Cabana, J.; Celestre, R.; Chao, W. L.; Kaznatcheev, K.; Kilcoyne, A. L. D.; Maia, F.; Marchesini, S.; *et al.* Chemical Composition Mapping with Nanometre Resolution by Soft X-Ray Microscopy. *Nat. Photonics* **2014**, *8*, 765–769.
16. Maroto, A.; Balasubramanian, K.; Burghard, M.; Kern, K. Functionalized Metallic Carbon Nanotube Devices for pH Sensing. *ChemPhysChem* **2007**, *8*, 220–223.
17. Shao, Y. Y.; Wang, J.; Wu, H.; Liu, J.; Aksay, I. A.; Lin, Y. H. Graphene Based Electrochemical Sensors and Biosensors: A Review. *Electroanal.* **2010**, *22*, 1027–1036.
18. Schedin, F.; Geim, A. K.; Morozov, S. V.; Hill, E. W.; Blake, P.; Katsnelson, M. I.; Novoselov, K. S. Detection of Individual Gas Molecules Adsorbed on Graphene. *Nat. Mater.* **2007**, *6*, 652–655.

19. Balasubramanian, K.; Zuccaro, L.; Kern, K. Tuneable Enhancement of Raman Scattering in Graphene-Nanoparticle Hybrids. *Adv. Funct. Mater.* **2014**, *24*, 6348–6358.
20. Kneipp, K.; Kneipp, H.; I, I.; Dasari, R. R.; Feld, M. S. Ultrasensitive Chemical Analysis by Raman Spectroscopy. *Chem. Rev.* **1999**, *99*, 2957.
21. Balasubramanian, K.; Burghard, M. Electrochemically Functionalized Carbon Nanotubes for Device Applications. *J. Mater. Chem.* **2008**, *18*, 3071–3083.
22. Sundaram, R. S.; Gomez-Navarro, C.; Balasubramanian, K.; Burghard, M.; Kern, K. Electrochemical Modification of Graphene. *Adv. Mater.* **2008**, *20*, 3050–3053.
23. Kneipp, J.; Kneipp, H.; Kneipp, K. SERS - a Single-Molecule and Nanoscale Tool for Bioanalytics. *Chem. Soc. Rev.* **2008**, *37*, 1052–1060.
24. Etchegoin, P. G.; Le Ru, E. C. A Perspective on Single Molecule SERS: Current Status and Future Challenges. *Phys. Chem. Chem. Phys.* **2008**, *10*, 6079–6089.
25. Zrimsek, A. B.; Henry, A. I.; Van Duyne, R. P. Single Molecule Surface-Enhanced Raman Spectroscopy without Nanogaps. *J. Phys. Chem. Lett.* **2013**, *4*, 3206–3210.
26. Willets, K. A. Super-Resolution Imaging of SERS Hot Spots. *Chem. Soc. Rev.* **2014**, *43*, 3854–3864.
27. Sonntag, M. D.; Pozzi, E. A.; Jiang, N.; Hersam, M. C.; Van Duyne, R. P. Recent Advances in Tip-Enhanced Raman Spectroscopy. *J. Phys. Chem. Lett.* **2014**, *5*, 3125–3130.
28. Chen, C.; Hayazawa, N.; Kawata, S. A 1.7 nm Resolution Chemical Analysis of Carbon Nanotubes by Tip-Enhanced Raman Imaging in the Ambient. *Nat. Commun.* **2014**, 5.
29. Stadler, J.; Schmid, T.; Zenobi, R. Nanoscale Chemical Imaging of Single-Layer Graphene. *ACS Nano* **2011**, *5*, 8442–8448.
30. Schmid, T.; Opilik, L.; Blum, C.; Zenobi, R. Nanoscale Chemical Imaging Using Tip-Enhanced Raman Spectroscopy: A Critical Review. *Angew. Chem., Int. Ed.* **2013**, *52*, 5940–5954.
31. Pozzi, E. A.; Sonntag, M. D.; Jiang, N.; Klingsporn, J. M.; Hersam, M. C.; Van Duyne, R. P. Tip-Enhanced Raman Imaging: An Emergent Tool for Probing Biology at the Nanoscale. *ACS Nano* **2013**, *7*, 885–888.
32. Hartschuh, A.; Qian, H.; Georgi, C.; Bohmler, M.; Novotny, L. Tip-Enhanced near-Field Optical Microscopy of Carbon Nanotubes. *Anal. Bioanal. Chem.* **2009**, *394*, 1787–1795.
33. Mauser, N.; Hartschuh, A. Tip-Enhanced near-Field Optical Microscopy. *Chem. Soc. Rev.* **2014**, *43*, 1248–1262.
34. Huth, F.; Chuvilin, A.; Schnell, M.; Amenabar, I.; Krutokhvostov, R.; Lopatin, S.; Hillenbrand, R. Resonant Antenna Probes for Tip-Enhanced Infrared near-Field Microscopy. *Nano Lett.* **2013**, *13*, 1065–1072.
35. Goss, K.; Peica, N.; Thomsen, C.; Maultzsch, J.; Schneider, C. M.; Meyer, C. Index Assignment of a Carbon Nanotube Rope Using Tip-Enhanced Raman Spectroscopy. *Phys. Status Solidi B* **2011**, *248*, 2577–2580.
36. Hartschuh, A.; Anderson, N.; Novotny, L. Near-Field Raman Spectroscopy Using a Sharp Metal Tip. *J. Microsc.* **2003**, *210*, 234–240.
37. Zhang, R.; Zhang, Y.; Dong, Z. C.; Jiang, S.; Zhang, C.; Chen, L. G.; Zhang, L.; Liao, Y.; Aizpurua, J.; Luo, Y.; *et al*. Chemical Mapping of a Single Molecule by Plasmon-Enhanced Raman Scattering. *Nature* **2013**, *498*, 82–86.
38. Yano, T.; Verma, P.; Saito, Y.; Ichimura, T.; Kawata, S. Pressure-Assisted Tip-Enhanced Raman Imaging at a Resolution of a Few Nanometres. *Nat. Photonics* **2009**, *3*, 473–477.
39. Anderson, N.; Hartschuh, A.; Novotny, L. Chirality Changes in Carbon Nanotubes Studied with near-Field Raman Spectroscopy. *Nano Lett.* **2007**, *7*, 577–582.
40. Peica, N.; Thomsen, C.; Maultzsch, J. Studying the Local Character of Raman Features of Single-Walled Carbon Nanotubes Along a Bundle Using TERS. *Nanoscale Res. Lett.* **2011**, *6*.
41. Georgi, C.; Hartschuh, A. Tip-Enhanced Raman Spectroscopic Imaging of Localized Defects in Carbon Nanotubes. *Appl. Phys. Lett.* **2010**, *97*, 143117-1−143117-3.
42. Hartschuh, A.; Sanchez, E. J.; Xie, X. S.; Novotny, L. High-Resolution near-Field Raman Microscopy of Single-Walled Carbon Nanotubes. *Phys. Rev. Lett.* **2003**, *90*, 095503-1−095503-4.
43. Amenabar, I.; Poly, S.; Nuansing, W.; Hubrich, E. H.; Govyadinov, A. A.; Huth, F.; Krutokhvostov, R.; Zhang, L. B.; Knez, M.; Heberle, J., *et al*. Structural Analysis and Mapping of Individual Protein Complexes by Infrared Nanospectroscopy. *Nat. Commun.* **2013**, 4.
44. Lu, F.; Jin, M. Z.; Belkin, M. A. Tip-Enhanced Infrared Nanospectroscopy *via* Molecular Expansion Force Detection. *Nat. Photonics* **2014**, *8*, 307–312.
45. Assmus, T.; Balasubramanian, K.; Burghard, M.; Kern, K.; Scolari, M.; Fu, N.; Myalitsin, A.; Mews, A. Raman Properties of Gold Nanoparticle-Decorated Individual Carbon Nanotubes. *Appl. Phys. Lett.* **2007**, *90*, 173109-1−173109-3.
46. Paulus, G. L. C.; Wang, Q. H.; Strano, M. S. Covalent Electron Transfer Chemistry of Graphene with Diazonium Salts. *Acc. Chem. Res.* **2013**, *46*, 160–170.
47. Balasubramanian, K.; Friedrich, M.; Jiang, C. Y.; Fan, Y. W.; Mews, A.; Burghard, M.; Kern, K. Electrical Transport and Confocal Raman Studies of Electrochemically Modified Individual Carbon Nanotubes. *Adv. Mater.* **2003**, *15*, 1515–1518.
48. Gao, M.; Huang, S. M.; Dai, L. M.; Wallace, G.; Gao, R. P.; Wang, Z. L. Aligned Coaxial Nanowires of Carbon Nanotubes Sheathed with Conducting Polymers. *Angew. Chem. Int. Ed.* **2000**, *39*, 3664–3667.
49. Huang, J. E.; Li, X. H.; Xu, J. C.; Li, H. L. Well-Dispersed Single-Walled Carbon Nanotube/Polyaniline Composite Films. *Carbon* **2003**, *41*, 2731–2736.
50. An, K. H.; Jeon, K. K.; Heo, J. K.; Lim, S. C.; Bae, D. J.; Lee, Y. H. High-Capacitance Supercapacitor Using a Nanocomposite Electrode of Single-Walled Carbon Nanotube and Polypyrrole. *J. Electrochem. Soc.* **2002**, *149*, A1058–A1062.
51. Dudin, P. V.; Unwin, P. R.; Macpherson, J. V. Electrochemical Nucleation and Growth of Gold Nanoparticles on Single-Walled Carbon Nanotubes: New Mechanistic Insights. *J. Phys. Chem. C* **2010**, *114*, 13241–13248.
52. Scolari, M.; Mews, A.; Fu, N.; Myalitsin, A.; Assmus, T.; Balasubramanian, K.; Burghard, M.; Kern, K. Surface Enhanced Raman Scattering of Carbon Nanotubes Decorated by Individual Fluorescent Gold Particles. *J. Phys. Chem. C* **2008**, *112*, 391–396.
53. Furukawa, Y.; Tazawa, S.; Fujii, Y.; Harada, I. Raman-Spectra of Polypyrrole and Its 2,5-C-13-Substituted and C-Deuterated Analogs in Doped and Undoped States. *Synth. Met.* **1988**, *24*, 329–341.
54. Faulques, E.; Wallnofer, W.; Kuzmany, H. Vibrational Analysis of Heterocyclic Polymers - a Comparative-Study of Polythiophene, Polypyrrole, and Polyisothianaphthene. *J. Chem. Phys.* **1989**, *90*, 7585–7593.
55. Doherty, M. D.; Murphy, A.; Pollard, R. J.; Dawson, P. Surface-Enhanced Raman Scattering from Metallic Nanostructures: Bridging the Gap between the near-Field and far-Field Responses. *Phys. Rev. X* **2013**, *3*, 011001-1−011001-12.
56. Zhao, L. L.; Jensen, L.; Schatz, G. C. Surface-Enhanced Raman Scattering of Pyrazine at the Junction between Two Ag-20 Nanoclusters. *Nano Lett.* **2006**, *6*, 1229–1234.
57. Le, H. N. T.; Bernard, M. C.; Garcia-Renaud, B.; Deslouis, C. Raman Spectroscopy Analysis of Polypyrrole Films as Protective Coatings on Iron. *Synth. Met.* **2004**, *140*, 287–293.
58. Liu, Y. C.; Hwang, B. J.; Jian, W. J.; Santhanam, R. *In Situ* Cyclic Voltammetry-Surface-Enhanced Raman Spectroscopy: Studies on the Doping-Undoping of Polypyrrole Film. *Thin Solid Films* **2000**, *374*, 85–91.
59. Krivan, E.; Visy, C. New Phenomena Observed during the Electrochemical Reduction of Conducting Polypyrrole Films. *J. Solid State Electrochem.* **2001**, *5*, 507–511.
60. Iost, R. M.; Crespilho, F. N.; Zuccaro, L.; Yu, H. K.; Wodtke, A. M.; Kern, K.; Balasubramanian, K. Enhancing the Electrochemical and Electronic Performance of CVD-Grown Graphene by Minimizing Trace Metal Impurities. *Chemelectrochem* **2014**, *1*, 2070–2074.
61. Mikat, J.; Orgzall, I.; Hochheimer, H. D. Raman Spectroscopy of Conducting Polypyrrole under High Pressure. *Phys. Rev. B* **2002**, *65*, 174202-1−174202-8.
62. Santos, M. J. L.; Brolo, A. G.; Girotto, E. M. Study of Polaron and Bipolaron States in Polypyrrole by *in Situ* Raman

Spectroelectrochemistry. *Electrochim. Acta* **2007**, *52*, 6141–6145.
63. Sadki, S.; Schottland, P.; Brodie, N.; Sabouraud, G. The Mechanisms of Pyrrole Electropolymerization. *Chem. Soc. Rev.* **2000**, *29*, 283–293.
64. Krivan, E.; Visy, C.; Kankare, J. Deprotonation and Dehydration of Pristine PPy/Ds Films During Open-Circuit Relaxation: An Ignored Factor in Determining the Properties of Conducting Polymers. *J. Phys. Chem. B* **2003**, *107*, 1302–1308.
65. Mcdermott, D. P. Vibrational Assignments and Normal-Coordinate Analyses of Gamma-Butyrolactone and 2-Pyrrolidinones. *J. Phys. Chem.* **1986**, *90*, 2569–2574.
66. Borodko, Y.; Humphrey, S. M.; Tilley, T. D.; Frei, H.; Somorjai, G. A. Charge-Transfer Interaction of Poly(Vinylpyrrolidone) with Platinum and Rhodium Nanoparticles. *J. Phys. Chem. C* **2007**, *111*, 6288–6295.
67. Fukushima, K.; Yamaji, M. Raman-Spectra of Compounds under Inversion Motions 0.4. N-Methyl-2-Pyrrolidone. *Bull. Chem. Soc. Jpn.* **1985**, *58*, 1495–1499.
68. Cheung, K. M.; Bloor, D.; Stevens, G. C. Characterization of Polypyrrole Electropolymerized on Different Electrodes. *Polymer* **1988**, *29*, 1709–1717.
69. Ghosh, S.; Bowmaker, G. A.; Cooney, R. P.; Seakins, J. M. Infrared and Raman Spectroscopic Studies of the Electrochemical Oxidative Degradation of Polypyrrole. *Synth. Met.* **1998**, *95*, 63–67.
70. Borodko, Y.; Habas, S. E.; Koebel, M.; Yang, P. D.; Frei, H.; Somorjai, G. A. Probing the Interaction of Poly-(Vinylpyrrolidone) with Platinum Nanocrystals by UV-Raman and FTIR. *J. Phys. Chem. B* **2006**, *110*, 23052–23059.
71. Novak, P. Limitations of Polypyrrole Synthesis in Water and Their Causes. *Electrochim. Acta* **1992**, *37*, 1227–1230.
72. Valmalette, J. C.; Tan, Z. Q.; Abe, H.; Ohara, S. Raman Scattering of Linear Chains of Strongly Coupled Ag Nanoparticles on SWCNTs. *Sci. Rep.* **2014**, *4*, 5238-1−5238-8.
73. Bernard, M. C.; Hugot-Le Goff, A. Quantitative Characterization of Polyaniline Films Using Raman Spectroscopy I: Polaron Lattice and Bipolaron. *Electrochim. Acta* **2006**, *52*, 595–603.
74. da Silva, J. E. P.; de Faria, D. L. A.; de Torresi, S. I. C.; Temperini, M. L. A. Influence of Thermal Treatment on Doped Polyaniline Studied by Resonance Raman Spectroscopy. *Macromolecules* **2000**, *33*, 3077–3083.
75. Cochet, M.; Louarn, G.; Quillard, S.; Boyer, M. I.; Buisson, J. P.; Lefrant, S. Theoretical and Experimental Vibrational Study of Polyaniline in Base Forms: Non-Planar Analysis. Part I. *J. Raman Spectrosc.* **2000**, *31*, 1029–1039.
76. Cochet, M.; Louarn, G.; Quillard, S.; Buisson, J. P.; Lefrant, S. Theoretical and Experimental Vibrational Study of Emeraldine in Salt Form. Part II. *J. Raman Spectrosc.* **2000**, *31*, 1041–1049.
77. Bernard, M. C.; de Torresi, S. C.; Hugot-Le Goff, A. *In Situ* Raman Study of Sulfonate-Doped Polyaniline. *Electrochim. Acta* **1999**, *44*, 1989–1997.
78. Pachauri, V.; Kern, K.; Balasubramanian, K. Field-Effect-Based Chemical Sensing Using Nanowire-Nanoparticle Hybrids: The Ion-Sensitive Metal-Semiconductor Field-Effect Transistor. *Appl. Phys. Lett.* **2013**, *102*, 023501.
79. Kurkina, T.; Vlandas, A.; Ahmad, A.; Kern, K.; Balasubramanian, K. Label-Free Detection of Few Copies of DNA with Carbon Nanotube Impedance Biosensors. *Angew. Chem., Int. Ed.* **2011**, *50*, 3710–3714.